
Enabling Binary Neural Network Training on the Edge

**Erwei Wang¹, James J. Davis¹, Daniele Moro², Piotr Zielinski², Claudiomir Coelho³,
Sat Chatterjee², Peter Y. K. Cheung¹, George A. Constantinides¹**

¹Imperial College London, ²Google, ³Palo Alto Networks

erweiw@acm.org

Abstract

The ever-growing computational demands of increasingly complex machine learning models frequently necessitate the use of powerful cloud-based infrastructure for their training. Binary neural networks are known to be promising candidates for on-device inference due to their extreme compute and memory savings over higher-precision alternatives. However, their existing training methods require the concurrent storage of high-precision activations for all layers, generally making learning on memory-constrained devices infeasible. In this paper, we demonstrate that the backward propagation operations needed for binary neural network training are strongly robust to quantization, thereby making on-the-edge learning with modern models a practical proposition. We introduce a low-cost binary neural network training strategy exhibiting sizable memory footprint and energy reductions while inducing little to no accuracy loss vs Courbariaux & Bengio’s standard approach. These resource decreases are primarily enabled through the retention of activations exclusively in binary format. Against the latter algorithm, our drop-in replacement sees coincident memory requirement and energy consumption drops of $2\text{--}6\times$, while reaching similar test accuracy in comparable time, across a range of small-scale models trained to classify popular datasets. We also demonstrate from-scratch ImageNet training of binarized ResNet-18, achieving a $3.12\times$ memory reduction. Such savings will allow for unnecessary cloud offloading to be avoided, reducing latency, increasing energy efficiency and safeguarding privacy.

1 Introduction

Although binary neural networks (BNNs) feature weights and activations with just single-bit precision, many models are able to reach accuracy indistinguishable from that of their higher-precision counterparts [Courbariaux and Bengio, 2016, Wang et al., 2019b]. Since BNNs are functionally complete, their limited precision does not impose an upper bound on achievable accuracy [Constantinides, 2019]. BNNs represent the ideal class of neural networks for edge inference, particularly for custom hardware implementation, due to their use of XNOR for multiplication: a fast and cheap operation to perform. Their use of compact weights also suits systems with limited memory and increases opportunities for caching, providing further potential performance boosts. FINN, the seminal BNN implementation for field-programmable gate arrays, reached the highest CIFAR-10 and SVHN classification rates to date at the time of its publication [Umuroglu et al., 2017].

Despite featuring binary forward propagation, existing BNN training approaches perform backward propagation using high-precision floating-point data types—typically `float32`—often making training infeasible on resource-constrained devices. The high-precision activations used between forward and backward propagation commonly constitute the largest proportion of the total memory footprint of a training run [Sohoni et al., 2019, Cai et al., 2020]. Moreover, backward propagation with high-precision gradients is costly, challenging the energy limitations of edge platforms.

Table 1: Applied approximations, where applicable, in low-cost neural network training works.

	Weights	Weight gradients	Activations	Activation gradients	Batch normalization
Zhou et al. [2016]	int6 ¹	int6	int6	int6	✗
Gruslys et al. [2016]	✗	✗	Recomputed ²	✗	✗
Ginsburg et al. [2017]	float16	float16	float16	float16	✗
Graham [2017]	✗	✗	int	✗	✗
Bernstein et al. [2018]	✗	bool	✗	✗	✗
Wu et al. [2018b]	✗	✗	✗	✗	ℓ_1
This work	bool	bool	bool	po2 ³	BNN-specific ℓ_1

¹ Arbitrary precision was supported, but significant accuracy degradation was observed below 6 bits.

² Activations were not retained between forward and backward propagation in order to save memory.

³ Power-of-two format comprising sign bit and exponent.

Our understanding of standard BNN training algorithms led to the following realization: high-precision activations and weight gradients should not be used since we are only concerned with weights and activations’ *signs*. In this paper, we present a low-memory, low-energy BNN training scheme based on this intuition featuring (i) binary activations only, facilitated through batch normalization modification, and (ii) matrix multiplication devoid of floating-point operations.

By increasing the viability of learning on the edge, this work will reduce the domain mismatch between training and inference—particularly in conjunction with federated learning [McMahan et al., 2017, Bonawitz et al., 2019]—and ensure privacy for sensitive applications [Agarwal et al., 2018]. Via the aggressive energy and memory footprint reductions they facilitate, our proposals will enable models to be trained without the network access reliance, latency and energy overheads or data divulgence inherent to cloud offloading. Herein, we make the following novel contributions.

- We conduct the first variable representation and lifetime analysis of the standard BNN training process introduced by Courbariaux and Bengio [2016]. We use this to identify opportunities for memory and energy savings through approximation.
- Via our proposed BNN-specific forward and backward batch normalization operations, we implement the first neural network training regime featuring all-binary activations. This significantly reduces the greatest constituent of a given training run’s total memory footprint.
- Furthermore, ours is the first neural network training scheme in which binary activations, binary weight gradients and power-of-two activation gradients are successfully combined. This aggregation allows us to eliminate energy-hungry floating-point matrix multiplication.
- We systematically evaluate the impact of each of these approximations, and provide a detailed characterization of our scheme’s memory and energy requirements vs accuracy.
- Against the standard approach, we report memory and energy reductions of up to $5.67\times$ and $4.53\times$, with little to no accuracy or convergence rate degradation, when training BNNs to classify MNIST, CIFAR-10 and SVHN. No hyperparameter tuning is required. We also show that the batch size used can be increased by up to $10\times$ while remaining within a given memory envelope, and even demonstrate the efficacy of ImageNet training as a hard target.
- We provide an open-source release of our training software, along with our memory and energy estimation tools, for the community to use and build upon¹. Our memory breakdown analysis represents a clear road map to further reductions in the future.

2 Related Work

The authors of all published works on BNN inference acceleration to date made use of high-precision floating-point data types during training [Courbariaux et al., 2015, Courbariaux and Bengio, 2016, Lin et al., 2017, Ghasemzadeh et al., 2018, Liu et al., 2018, Wang et al., 2019a, 2020, Umuroglu et al., 2020, He et al., 2020, Liu et al., 2020]. There is precedent, however, for the use of quantization when

¹<https://github.com/awai54st/Enabling-Binary-Neural-Network-Training-on-the-Edge>

training non-binary networks, as we show in Table 1 via side-by-side comparison of the approximation approaches taken in those works along with those in ours.

The effects of quantizing the gradients of models with high-precision data, either fixed or floating point, have been studied extensively. Zhou et al. [2016] and Wu et al. [2018a] trained networks with fixed-point weights and activations using fixed-point gradients, reporting no accuracy loss for AlexNet classifying ImageNet with gradients wider than five bits. Wen et al. [2017] and Bernstein et al. [2018] focused solely on aggressive weight gradient quantization, aiming to reduce communication costs for distributed learning. Weight gradients were losslessly quantized into ternary and binary formats, respectively, with forward propagation and activation gradients kept at high precision. In this work, we make the novel observations that activation gradient dynamic range is more important than precision, and that BNNs are more robust to approximation during training than higher-precision networks. We thus propose a data representation scheme more aggressive than all of the aforementioned works combined, delivering large memory and energy savings with near-lossless performance.

An intuitive method to lower the memory footprint of training is to simply reduce the batch size. However, doing so generally leads to increased total training time due to reduced memory reuse [Sohoni et al., 2019]. The methods we propose in this paper do not conflict with batch size tuning, and further allow the use of large batches while remaining within the memory limits of edge devices.

Gradient checkpointing—the recomputation of activations during backward propagation—has been proposed as a method to reduce the memory consumption of training [Chen et al., 2016, Gruslys et al., 2016]. Such methods introduce additional forward passes, however, and so increase each run’s duration and energy cost. Graham [2017] and Chakrabarti and Moseley [2019] saved memory during training by buffering activations in low-precision formats, achieving comparable accuracy to all-float32 baselines. Wu et al. [2018b] and Hoffer et al. [2018] reported reduced computational costs via ℓ_1 batch normalization. Finally, Helwegen et al. [2019] asserted that the use of both trainable weights and momenta is superfluous in BNN optimizers, proposing a weightless BNN-specific optimizer, Bop, able to reach the same level of accuracy as Adam. We took inspiration from these works in locating sources of redundancy present in standard BNN training schemes, and propose BNN-specific modifications to ℓ_1 batch normalization allowing for activation quantization all the way down to binary, thus saving memory and energy without increasing latency.

3 Standard Training Flow

For simplicity of exposition, we assume the use of a multi-layer perceptron (MLP), although the presence of convolutional layers would not change any of the principles that follow. Let \mathbf{W}_l and \mathbf{X}_l denote matrices of weights and activations, respectively, in the network’s l^{th} layer, with $\partial\mathbf{W}_l$ and $\partial\mathbf{X}_l$ being their gradients. For \mathbf{W}_l , rows and columns span input and output channels, respectively, while for \mathbf{X}_l they represent images and channels. Henceforth, we use decoration to indicate low-precision data encoding, with $\hat{\bullet}$ and $\tilde{\bullet}$ respectively denoting binary and power-of-two.

Figure 1 shows the training graph of a fully connected binary layer. A detailed description of the standard BNN training procedure introduced by Courbariaux and Bengio [2016] for each batch of B training samples, which we henceforth refer to as a *step*, is provided in Algorithm 1. Therein, “ \odot ” signifies element-wise multiplication. For brevity, we omit some of the intricacies of the baseline implementation—lack of first-layer quantization, use of a final softmax layer and the inclusion of weight gradient cancellation [Courbariaux and Bengio, 2016]—as these standard BNN practices are not impacted by our work. We initialize weights as outlined by Glorot and Bengio [2010].

Many authors have established that BNNs require batch normalization in order to avoid gradient explosion [Alizadeh et al., 2018, Sari et al., 2019, Qin et al., 2020], and our early experiments

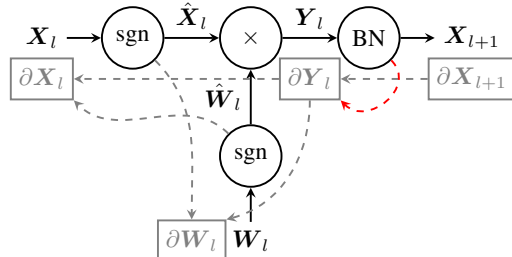


Figure 1: Standard BNN training graph for fully connected layer l . “sgn”, “ \times ” and “BN” are sign, matrix multiplication and batch normalization operations. Forward propagation dependencies are shown with solid lines; those for backward passes are dashed. High-precision activations must be retained due to the dependency in red.

Algorithm 1 Standard BNN training step.

```

1: for  $l \leftarrow \{1, \dots, L-1\}$  do            $\triangleright$  Forward
2:    $\hat{\mathbf{X}}_{l+1} \leftarrow \text{sgn}(\mathbf{X}_{l+1})$ 
3:    $\hat{\mathbf{W}}_l \leftarrow \text{sgn}(\mathbf{W}_l)$ 
4:    $\mathbf{Y}_l \leftarrow \hat{\mathbf{X}}_l \hat{\mathbf{W}}_l$ 
5:   for  $m \leftarrow \{1, \dots, M_l\}$  do            $\triangleright$  Norm.
6:      $\mathbf{x}_{l+1}^{(m)} \leftarrow \frac{\mathbf{y}_l^{(m)} - \mu(\mathbf{y}_l^{(m)})}{\sigma(\mathbf{y}_l^{(m)})} + \beta_l^{(m)}$ 
7:
8: for  $l \leftarrow \{L-1, \dots, 1\}$  do            $\triangleright$  Backward
9:   for  $m \leftarrow \{1, \dots, M_l\}$  do            $\triangleright$  Norm.
10:     $\mathbf{v} \leftarrow \frac{1}{\sigma(\mathbf{y}_l^{(m)})} \partial \mathbf{x}_{l+1}^{(m)}$ 
11:     $\partial \mathbf{y}_l^{(m)} \leftarrow \mathbf{v} - \mu(\mathbf{v}) -$ 
         $\mu \left( \mathbf{v} \odot \left[ \mathbf{x}_{l+1}^{(m)} \right] \right) \left[ \mathbf{x}_{l+1}^{(m)} \right]$ 
12:     $\partial \beta_l^{(m)} \leftarrow \sum \partial \mathbf{x}_{l+1}^{(m)}$ 
13:
14:    $\partial \mathbf{X}_l \leftarrow \partial \mathbf{Y}_l \hat{\mathbf{W}}_l^T$ 
15:    $\partial \mathbf{W}_l \leftarrow \hat{\mathbf{X}}_l^T \partial \mathbf{Y}_l$ 
16:
17: for  $l \leftarrow \{1, \dots, L-1\}$  do            $\triangleright$  Update
18:    $\mathbf{W}_l \leftarrow \text{Optimize}(\mathbf{W}_l, \partial \mathbf{W}_l, \eta)$ 
19:    $\beta_l \leftarrow \text{Optimize}(\beta_l, \partial \beta_l, \eta)$ 
20:  $\eta \leftarrow \text{LearningRateSchedule}(\eta)$ 

```

Algorithm 2 Proposed BNN training step.

```

1: for  $l \leftarrow \{1, \dots, L-1\}$  do            $\triangleright$  Forward
2:    $\hat{\mathbf{X}}_{l+1} \leftarrow \text{sgn}(\mathbf{X}_{l+1})$ 
3:    $\hat{\mathbf{W}}_l \leftarrow \text{sgn}(\mathbf{W}_l)$ 
4:    $\mathbf{Y}_l \leftarrow \hat{\mathbf{X}}_l \hat{\mathbf{W}}_l$ 
5:   for  $m \leftarrow \{1, \dots, M_l\}$  do            $\triangleright$  Norm.
6:      $\mathbf{x}_{l+1}^{(m)} \leftarrow \frac{\mathbf{y}_l^{(m)} - \mu(\mathbf{y}_l^{(m)})}{\| \mathbf{y}_l^{(m)} - \mu(\mathbf{y}_l^{(m)}) \|_1 / B} + \beta_l^{(m)}$ 
7:      $\alpha_{l+1}^{(m)} \leftarrow \| \mathbf{x}_{l+1}^{(m)} \|_1 / B$ 
8: for  $l \leftarrow \{L-1, \dots, 1\}$  do            $\triangleright$  Backward
9:   for  $m \leftarrow \{1, \dots, M_l\}$  do            $\triangleright$  Norm.
10:     $\mathbf{v} \leftarrow \frac{1}{\| \mathbf{y}_l^{(m)} - \mu(\mathbf{y}_l^{(m)}) \|_1 / B} \partial \mathbf{x}_{l+1}^{(m)}$ 
11:     $\partial \mathbf{y}_l^{(m)} \leftarrow \mathbf{v} - \mu(\mathbf{v}) -$ 
         $\mu \left( \mathbf{v} \odot \left[ \hat{\mathbf{x}}_{l+1}^{(m)} \alpha_{l+1}^{(m)} \right] \right) \left[ \hat{\mathbf{x}}_{l+1}^{(m)} \right]$ 
12:     $\partial \beta_l^{(m)} \leftarrow \sum \partial \mathbf{x}_{l+1}^{(m)}$ 
13:     $\partial \hat{\mathbf{Y}}_l \leftarrow \text{po2}(\partial \mathbf{Y}_l)$ 
14:    $\partial \mathbf{X}_l \leftarrow \partial \hat{\mathbf{Y}}_l \hat{\mathbf{W}}_l^T$ 
15:    $\partial \mathbf{W}_l \leftarrow \hat{\mathbf{X}}_l^T \partial \hat{\mathbf{Y}}_l$ 
16:    $\partial \hat{\mathbf{W}}_l \leftarrow \text{sgn}(\partial \mathbf{W}_l)$ 
17: for  $l \leftarrow \{1, \dots, L-1\}$  do            $\triangleright$  Update
18:    $\mathbf{W}_l \leftarrow \text{Optimize}(\mathbf{W}_l, \partial \hat{\mathbf{W}}_l / \sqrt{M_{l-1}}, \eta)$ 
19:    $\beta_l \leftarrow \text{Optimize}(\beta_l, \partial \beta_l, \eta)$ 
20:  $\eta \leftarrow \text{LearningRateSchedule}(\eta)$ 

```

$\hat{\bullet}$ and $\tilde{\bullet}$ denote binary and power-of-two encoding, respectively. Our refinements of Algorithm 1 are shown in red. Dashed boxes highlight Algorithm 2’s lack of dependence on high-precision activations. Detailed description of our approach can be found in Section 5.

confirmed this to indeed be the case. We thus apply it as standard. Matrix products \mathbf{Y}_l are channel-wise batch-normalized across each layer’s M_l output channels (Algorithm 1 lines 5–6) to form the subsequent layer’s inputs, \mathbf{X}_{l+1} . β constitutes the batch normalization biases. We forgo trainable scaling factors, commonly denoted γ ; these are of irrelevance to BNNs since their activations are binarized during forward propagation (line 2).

As emphasized in both Figure 1 and Algorithm 1 (line 11), BNN training requires *high-precision* storage of the entire network’s activations. The addressment of this forms our key contribution.

4 Variable Analysis

In order to quantify the potential gains from approximation, we conducted a variable representation and lifetime analysis of Algorithm 1 following the approach taken by Sohoni et al. [2019]. Table 2 lists the properties of all variables in Algorithm 1, with each variable’s contributions to the total footprint shown for a representative example. Variables are divided into two classes: those that must remain in memory between computational phases (forward propagation, backward propagation and weight update), and those that need not. This is of pertinence since, for those in the latter category, only the largest layer’s contribution counts towards the total memory occupancy. For example, $\partial \mathbf{X}_l$ is read during the backward propagation of layer $l-1$ only, thus $\partial \mathbf{X}_{l-1}$ can safely overwrite $\partial \mathbf{X}_l$ for efficiency. Additionally, \mathbf{Y} and $\partial \mathbf{X}$ are shown together since they are equally sized and only need to reside in memory during the forward and backward pass for each layer, respectively.

Table 2: Memory-related properties of variables used during training. In order to obtain these exemplary memory quantities, BinaryNet was trained for CIFAR-10 classification with Adam.

Variable	Per-layer lifetime ¹	Standard training			Proposed training		
		Data type	Size (MiB)	%	Data type	Size (MiB)	Saving (×)
X	✗	float32	111.33	26.18	bool	3.48	32.00
$\partial X, Y^2$	✓	float32	50.00	11.76	float16	25.00	2.00
$\mu(y_l), \sigma(y_l)$	✗	float32	0.03	0.00	float16	0.02	2.00
∂Y	✓	float32	50.00	11.76	po2_5 ³	7.81	6.40
W	✗	float32	53.49	12.58	float16	26.74	2.00
∂W	✗	float32	53.49	12.58	bool	1.67	32.00
$\beta, \partial \beta$	✗	float32	0.03	0.00	float16	0.02	2.00
Momenta	✗	float32	106.98	25.15	float16	53.49	2.00
Total			425.35	100.00		118.23	3.60

¹ ✓ indicates that a variable does not need to be retained between forward, backward or update phases.

² ∂X and Y can share memory since they are equally sized and have non-overlapping lifetime.

³ 5-bit power-of-two format with 4-bit exponent.

5 Low-Cost BNN Training

As shown in Table 2, all variables within the standard BNN training flow use `float32` representation. In the subsections that follow, we detail the application of aggressive approximation specifically tailored to BNN training. Further to this, and in line with the observation by many authors that `float16` can be used for ImageNet training without inducing accuracy loss [Ginsburg et al., 2017, Wang et al., 2018, Micikevicius et al., 2018], we also switch all remaining variables to this format. Our final training procedure is captured in Algorithm 2, with modifications from Algorithm 1 in red and the corresponding data representations used shown in Table 2. We provide both theoretical evidence and training curves for all of our experiments in Appendix A to show that our proposed changes do not cause material convergence rate degradation.

5.1 High-Precision Activation Elimination via Batch Normalization Approximation

Analysis of the backward pass of Algorithm 1 reveals conflicting requirements for the precision of X . When computing weight gradients ∂W (line 15), only binary activations \hat{X} are needed. For the batch normalization training (lines 9–12), however, high-precision X is used. The latter occurrences are highlighted with dashed boxes. As was shown in Table 2, the storage of X between forward and backward propagation constitutes the single largest portion of the algorithm’s total memory. If we are able to use \hat{X} in place of X for these operations, there will be no need for this high-precision activation retention, significantly reducing memory footprint as a result. We achieve this as follows.

Step 1: ℓ_1 normalization. Standard batch normalization sees channel-wise ℓ_2 normalization performed on each layer’s centralized activations. Since batch normalization is immediately followed by binarization in BNNs, however, we argue that less-costly ℓ_1 normalization is good enough in this circumstance. Replacement of batch normalization’s backward propagation operation with our ℓ_1 norm-based version sees lines 10–11 of Algorithm 1 swapped with (1), where B is the batch size. Not only does our use of ℓ_1 batch normalization eliminate all squares and square roots, it also transforms one occurrence of $x_{l+1}^{(m)}$ into its binary form.

$$v \leftarrow \frac{1}{\|y_l^{(m)} - \mu(y_l^{(m)})\|_1 / B} \partial x_{l+1}^{(m)} \quad \partial y_l^{(m)} \leftarrow v - \mu(v) - \mu(v \odot x_{l+1}^{(m)}) \hat{x}_{l+1}^{(m)} \quad (1)$$

Step 2: BNN-specific approximation. Since ∂Y is quantized immediately after its calculation (Algorithm 2 line 13), we hypothesize that it should be robust to approximation. Consequently, we replace the remaining $x_{l+1}^{(m)}$ term in (1) with the product of its signs and mean magnitude— $\hat{x}_{l+1}^{(m)} \alpha_{l+1}^{(m)}$ —where $\alpha_{l+1}^{(m)}$ is calculated during the forward propagation phase (line 7).

Our complete batch normalization training functions are shown on lines 9–12 of Algorithm 2. As again highlighted within dashed boxes, these only require the storage of binary $\hat{\mathbf{X}}$ along with pre-computed layer- and channel-wise mean magnitudes. With elements of \mathbf{X} now binarized, we reduce its memory cost by $32\times$ and also save energy thanks to the corresponding memory traffic reduction.

5.2 Gradient Quantization

We also propose a gradient quantization scheme leading to further memory and energy savings. Combined with activation binarization, this enables us to eliminate floating-point matrix multiplication.

Binarized weight gradients. Intuitively, BNNs should be particularly robust to weight gradient binarization since their weights only constitute signs. On line 16 of Algorithm 2, therefore, we quantize and store weight gradients in binary format, $\partial\hat{\mathbf{W}}$, for use during weight update. During that phase, we attenuate the gradients by $\sqrt{N_l}$, where N_l is layer l ’s fan-in, to reduce the learning rate and prevent premature weight clipping as advised by Sari et al. [2019] (line 18). Since fully connected layers are used as an example in Algorithm 2, $N_l = M_{l-1}$ in this instance.

Table 2 shows that, with binarization, the portion of our exemplary training run’s memory consumption attributable to weight gradients dropped from 53.49 to just 1.67 MiB, leaving the scarce resources available for more quantization-sensitive variables such as \mathbf{W} and momenta. Energy consumption will also decrease due to the associated reduction in memory traffic.

Power-of-two activation gradients. The tolerance of BNN training to weight gradient binarization further suggests that activation gradients can be aggressively approximated without causing significant accuracy loss. Unlike previous proposals, in which activation gradients were quantized into fixed- or block floating-point formats [Zhou et al., 2016, Wu et al., 2018a], we hypothesize that power-of-two representation is more suitable due to their typically high inter-channel variance. This is a similar observation to that made by Lai et al. [2017], who explained, with empirical support, that preservation of range is more important than precision for weights.

We define power-of-two quantization into k -bit “po2_k” format as $\text{po2}_k(\bullet) = \text{sgn}(\bullet) \odot 2^{\exp(\bullet)-b}$, comprising a sign bit and $k-1$ -bit exponent $\exp(\bullet) = \max(-2^{k-2}, [\log_2(\bullet) + b])$ with bias $b = 2^{k-2} - 1 - [\log_2(\|\bullet\|_\infty)]$. Square brackets signify rounding to the nearest integer. With b , we scale $\exp(\bullet)$ layer-wise to make efficient use of its dynamic range. This is applied to quantize matrix product gradients $\partial\mathbf{Y}_l$ on line 13 of Algorithm 2. We experimented with varying power-of-two gradient width, from two to eight bits, generally finding $k = 5$ to result in high compression while inducing little loss in accuracy. We thus used $k = 5$ as standard. While we elected not to similarly approximate $\partial\mathbf{X}$ due to its use in the computation of quantization-sensitive β , our use of $\partial\tilde{\mathbf{Y}} = \text{po2}(\partial\mathbf{Y})$ nevertheless leads to sizeable reductions in total memory footprint.

Our employment of power-of-two representation for $\partial\mathbf{Y}$ further allows us to reduce the energy consumption associated with lines 14–15 of Algorithm 2, for both of which we now have one binary and one power-of-two operand. Assuming that the target training platform has native support for only 32-bit fixed- and floating-point arithmetic, these matrix multiplications can be computed by (i) converting powers-of-two into `int32`s via shifts, (ii) performing sign-flips and (iii) accumulating the `int32` outputs. This consumes far less energy than standard training’s all-`float32` equivalent.

6 Evaluation

We implemented our BNN training method using Keras and TensorFlow, and experimented with the small-scale MNIST, CIFAR-10 and SVHN datasets, as well as large-scale ImageNet, using a range of network models. Our baseline for comparison was the standard BNN training method introduced by Courbariaux and Bengio [2016], and we followed those authors’ practice of reporting the highest test accuracy achieved in each run. Energy consumption results were obtained using the inference energy estimator from QKeras [Coelho Jr. et al., 2020], which we extended to also estimate the energy consumption of training. This tool assumes the use of an in-order processor fabricated on a 45 nm process and a cacheless memory hierarchy, as modeled by Horowitz [2014], resulting in high-level, platform-agnostic energy estimates useful for relative comparison. Note that we did not tune hyperparameters, thus it is likely that higher accuracy than we report is achievable.

Table 3: Test accuracy, memory footprint and per-batch energy consumption of the standard and proposed training schemes for a variety of models and datasets using the Adam optimizer.

Model (Dataset)	Top-1 test accuracy			Memory			Energy/batch		
	Std (%)	Prop. (%)	Δ (pp)	Std (MiB)	Prop. (MiB)	Saving (\times)	Std. (mJ)	Prop. (mJ)	Saving (\times)
MLP (MNIST)	98.24	96.83	-1.41	7.40	2.56	2.89	2.40	0.97	2.48
CNV (CIFAR-10)	82.67	82.31	-0.36	128.33	27.13	4.73	144.24	52.61	2.74
CNV (SVHN)	96.37	94.22	-2.15	128.33	27.13	4.73	144.24	52.61	2.74
BinaryNet (CIFAR-10)	89.81	88.36	-1.45	425.31	118.21	3.60	855.41	196.26	4.36
BinaryNet (SVHN)	97.40	95.78	-1.62	425.31	118.21	3.60	855.41	196.26	4.36

6.1 Small-Scale Datasets

For MNIST we evaluated using a five-layer MLP—henceforth simply denoted “MLP”—with 256 neurons per hidden layer, and CNV [Umuroglu et al., 2017] and BinaryNet [Courbariaux and Bengio, 2016] for both CIFAR-10 and SVHN. We used three popular BNN optimizers: Adam [Kingma and Ba, 2015], stochastic gradient descent (SGD) with momentum and Bop [Helwegen et al., 2019]. While all three function reliably with our training scheme, we used Adam by default due to its stability. Experimental setup minutiae can be found in Appendix B.1.

Our choice of quantization targets primarily rested on the intuition that BNNs should be more robust to approximation in backward propagation than their higher-precision counterparts. To illustrate that this is indeed the case, we compared our method’s loss when applied to BNNs vs float32 networks with identical topologies and hyperparameters. As shown in Table 1 of Appendix C, significantly higher accuracy degradation was observed for the non-binary networks, as expected. While our proposed BNN training method does exhibit limited accuracy degradation—a geomean drop of 1.21 percentage points (pp) for the examples given in Table 3—this comes in return for simultaneous geomean memory and energy savings of $3.66\times$ and $3.09\times$, respectively. It is also interesting to note that the reductions achievable for a given dataset depend on the model used. This observation is largely orthogonal to our work: by applying our approach to the training of a more appropriately chosen model, one can obtain the advantages of both optimized network selection and training.

In order to explore the impacts of the various facets of our scheme, we applied them sequentially while training BinaryNet to classify CIFAR-10 with multiple optimizers. As shown in Table 4, choices of data type, optimizer and batch normalization implementation lead to tradeoffs against performance and resource costs. Major memory savings are attributable to the use of float16 variables and through the high-precision activation elimination our ℓ_1 norm-based batch normalization facilitates. The bulk of our scheme’s energy savings come from the power-of-two representation of $\partial\mathbf{Y}$, which eliminates floating-point operations from lines 14–15 of Algorithm 2. We also evaluated the quantization of $\partial\mathbf{Y}$ into five-bit layer-wise block floating-point format, denoted “int5” in Table 4 since the individual elements are fixed-point values. With this encoding, significantly higher accuracy loss was observed than when $\partial\mathbf{Y}$ was quantized into the proposed, equally sized power-of-two format, confirming that representation of this variable’s range is indeed more important than its precision.

Figure 2 shows the memory footprint savings from our proposed BNN training method for different optimizers and batch sizes, again for BinaryNet with the CIFAR-10 dataset. Across all of these, we achieved a geomean reduction of $4.86\times$. Also observable from Figure 2 is that, for all three optimizers, movement from the standard to our proposed BNN training allows the batch size used to increase by $10\times$, facilitating faster completion, without a material increase in memory consumption. With respect to energy, we saw an estimated geomean $4.49\times$ reduction, split into contributions attributable to arithmetic operations and memory traffic of $18.27\times$ and $1.71\times$. Figure 2 also shows that test accuracy does not drop significantly due to our approximations. With Adam, there were small drops (geomean 0.87 pp), while with SGD and Bop we actually saw modest improvements.

Table 4: Accuracy, memory and energy impacts of moving from standard to proposed data representations with BinaryNet and CIFAR-10. We include block floating-point $\partial\mathbf{X}$ to illustrate the importance of its dynamic range over precision. Pareto-optimal points for each optimizer are bolded.

Optimizer	Data type		Batch norm.	Top-1 test accuracy		Memory saving (\times) ¹	Energy saving (\times) ¹
	$\partial\mathbf{W}$	$\partial\mathbf{Y}$		%	Δ (pp) ¹		
Adam	float32	float32	ℓ_2	88.74	–	–	–
	float16	float16	ℓ_2	88.71	–0.03	2.00	1.09
	bool	float16	ℓ_2	87.93	–0.81	2.27	1.10
	bool	int5 ²	ℓ_2	81.12	–7.62	2.50	4.32
	bool	po2_5	ℓ_2	89.47	0.73	2.50	4.01
	bool	po2_5	ℓ_1	87.64	–1.10	2.50	4.01
	bool	po2_5	BNN-spec. ℓ_1	88.59	–0.15	3.60	4.36
SGD with momentum	float32	float32	ℓ_2	88.52	–	–	–
	float16	float16	ℓ_2	88.54	0.02	2.00	1.09
	bool	float16	ℓ_2	87.35	–1.17	2.31	1.10
	bool	int5	ℓ_2	81.89	–6.63	2.59	4.40
	bool	po2_5	ℓ_2	89.08	0.56	2.59	4.06
	bool	po2_5	ℓ_1	88.69	0.17	2.59	4.06
	bool	po2_5	BNN-spec. ℓ_1	87.45	–1.07	4.07	4.45
Bop	float32	float32	ℓ_2	91.38	–	–	–
	float16	float16	ℓ_2	91.36	–0.02	2.00	1.09
	bool	float16	ℓ_2	90.54	–0.84	2.37	1.10
	bool	int5	ℓ_2	40.55	–50.83	2.72	4.48
	bool	po2_5	ℓ_2	89.34	–2.04	2.72	4.11
	bool	po2_5	ℓ_1	87.81	–3.57	2.72	4.11
	bool	po2_5	BNN-spec. ℓ_1	86.28	–5.10	4.92	4.53

¹ Baseline: float32 $\partial\mathbf{W}$ and $\partial\mathbf{X}$ with standard (ℓ_2) batch normalization.

² 5-bit fixed-point elements of layer-wise block floating-point format.

Table 5: Test accuracy, memory footprint and per-batch energy consumption of the standard and our proposed training schemes for ResNetE-18 classifying ImageNet with Adam used for optimization.

Approximations	Top-1 test accuracy		Memory		Energy/batch	
	%	Δ (pp) ¹	GiB	Saving (\times) ¹	J	Saving (\times) ¹
None	58.57	–	57.84	–	185.08	–
All-bfloat16	58.55	0.02	29.32	1.97	162.41	1.14
bool $\partial\mathbf{W}$ only	57.30	–1.27	57.80	1.00	185.08	1.00
po2_8 $\partial\mathbf{Y}$ only	29.56	–29.01	57.84	1.00	116.06	1.59
ℓ_1 batch norm. only	57.34	–1.23	57.84	1.00	185.08	1.00
Proposed batch norm. only	57.25	–1.32	35.59	1.63	176.87	1.05
Final combination²	56.32	–2.25	18.54	3.12	158.44	1.17

¹ Baseline: approximation-free training.

² bool $\partial\mathbf{W}$ and bfloat16 remaining variables with proposed batch normalization.

6.2 ImageNet

We also trained ResNetE-18, a mixed-precision model with most convolutional layers binarized [Bethge et al., 2019], to classify ImageNet. ResNetE-18 represents an exemplary instance within a broad class of ImageNet-capable networks, thus similar results should be achievable for models with which it shares architectural features. Setup specifics can be found in Appendix B.2.

We show the performance of this network and dataset when applying each of our proposed approximations in turn, as well as with the combination we found to work best, in Table 5. Since the Tensor Processing Units we used here natively support bfloat16 rather than float16, we switched to the

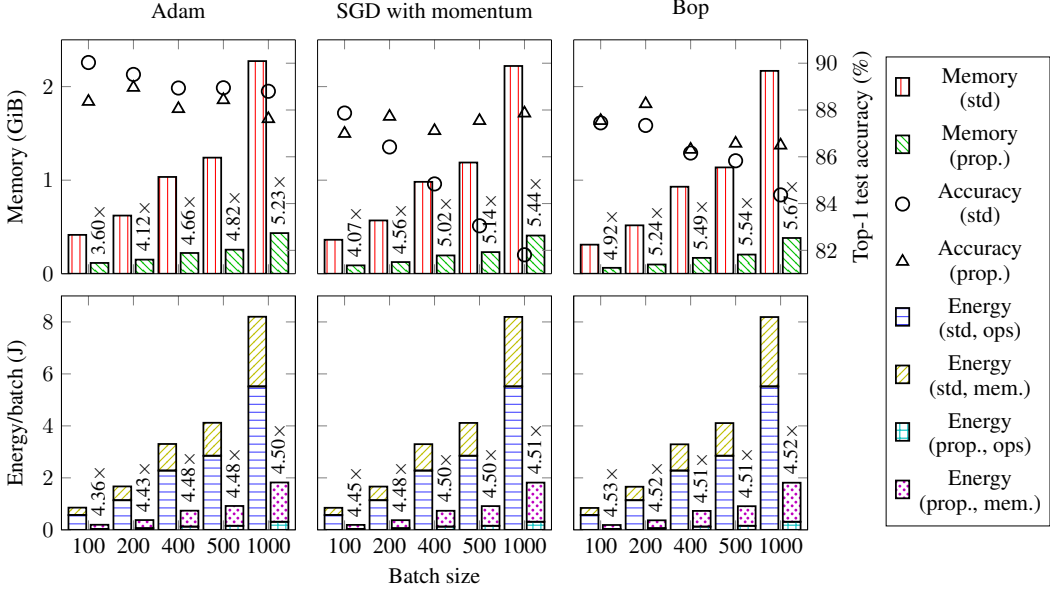


Figure 2: Batch size vs training memory footprint, achieved test accuracy and per-batch training energy consumption for BinaryNet with CIFAR-10. The upper plots show memory and accuracy results for the standard and our proposed training flows. In the lower plots, total energy is split into compute- and memory-related components. Annotations show reductions vs the standard approach.

former for these experiments. Where `bf100` variables were used, these were employed across all layers; the remaining approximations were applied only to binary layers. Despite increasing the precision of our power-of-two quantized ∂Y by moving from $k = 5$ to 8, this scheme unfortunately induced significant accuracy degradation, suggesting incompatibility with large-scale datasets. Consequently, we dispelled it for our final experiment, which saw our remaining approximations deliver memory and energy reductions of $3.12\times$ and $1.17\times$ in return for a 2.25 pp drop in test accuracy. While these savings are smaller than those for our small-scale experiments, we note that ResNetE-18's first convolutional layer is both its largest and is non-binary, thus its activation storage dwarfs that of the remaining layers. We also remark that, while ~ 2 pp accuracy drops may not be acceptable for some application deployments, sizable training resource reductions are otherwise achievable.

We acknowledge that dataset storage requirements likely render ImageNet training on edge platforms infeasible, and that network fine-tuning is a task more commonly deployed on devices of such scale. However, given that the accuracy changes and resource savings we report for more challenging, from-scratch training are favorable and reasonably consistent across a wide range of use-cases, we have confidence that positive results are readily achievable for fine-tuning as well. Nevertheless, our ImageNet proof of concept confirms the efficacy of large-scale neural network training on the edge.

7 Conclusion

In this paper, we introduced the first neural network training scheme tailored specifically to BNNs. Moving first to 16-bit floating-point representation, we selectively and opportunistically approximated beyond this based on careful analysis of the standard training algorithm presented by Courbariaux and Bengio [2016]. With a comprehensive evaluation conducted across multiple models, datasets, optimizers and batch sizes, we showed the generality of our approach and reported significant memory and energy reductions vs the prior art, challenging the notion that the resource constraints of edge platforms present insurmountable barriers to on-device learning. In the future, we will explore the potential of our training approximations in the custom hardware domain, within which we expect there to be vast energy-saving opportunity through the design of tailor-made arithmetic operators.

Acknowledgments

The authors are grateful for the support of the United Kingdom EPSRC (grant numbers EP/P010040/1 and EP/S030069/1). They also wish to thank Sergey Ioffe and Michele Covell for their helpful suggestions.

References

Naman Agarwal, Ananda Theertha Suresh, Felix Yu, Sanjiv Kumar, and H. Brendan McMahan. CpSGD: Communication-efficient and differentially-private distributed SGD. In *International Conference on Neural Information Processing Systems*, 2018.

Milad Alizadeh, Javier Fernández-Marqués, Nicholas D. Lane, and Yarin Gal. An empirical study of binary neural networks’ optimisation. In *International Conference on Learning Representations*, 2018.

Jeremy Bernstein, Yu-Xiang Wang, Kamyar Azizzadenesheli, and Animashree Anandkumar. SignSGD: Compressed optimisation for non-convex problems. In *International Conference on Machine Learning*, 2018.

Joseph Bethge, Haojin Yang, Marvin Bornstein, and Christoph Meinel. Back to simplicity: How to train accurate BNNs from scratch? *arXiv preprint arXiv:1906.08637*, 2019.

Keith Bonawitz, Hubert Eichner, Wolfgang Grieskamp, Dzmitry Huba, Alex Ingerman, Vladimir Ivanov, Chloe Kiddon, Jakub Konečný, Stefano Mazzocchi, H. Brendan McMahan, Timon van Overveldt, David Petrou, Daniel Ramage, and Jason Roselander. Towards federated learning at scale: System design. In *Conference on Machine Learning and Systems*, 2019.

Han Cai, Chuang Gan, Ligeng Zhu, and Song Han. Tiny Transfer Learning: Towards memory-efficient on-device learning. In *IEEE Conference on Computer Vision and Pattern Recognition*, 2020.

Ayan Chakrabarti and Benjamin Moseley. Backprop with approximate activations for memory-efficient network training. In *Advances in Neural Information Processing Systems*, 2019.

Tianqi Chen, Bing Xu, Chiyuan Zhang, and Carlos Guestrin. Training deep nets with sublinear memory cost. *arXiv preprint arXiv:1604.06174*, 2016.

Claudionor N. Coelho Jr., Aki Kuusela, Hao Zhuang, Thea Arrestad, Vladimir Loncar, Jennifer Ngadiuba, Maurizio Pierini, and Sioni Summers. Ultra low-latency, low-area inference accelerators using heterogeneous deep quantization with QKeras and hls4ml. *arXiv preprint arXiv:2006.10159*, 2020.

George A. Constantinides. Rethinking arithmetic for deep neural networks. *Philosophical Transactions of the Royal Society A*, 378(2166), 2019.

Matthieu Courbariaux and Yoshua Bengio. BinaryNet: Training deep neural networks with weights and activations constrained to +1 or -1. *arXiv preprint arXiv:1602.02830*, 2016.

Matthieu Courbariaux, Yoshua Bengio, and Jean-Pierre David. BinaryConnect: Training deep neural networks with binary weights during propagations. In *Conference on Neural Information Processing Systems*, 2015.

Mohammad Ghasemzadeh, Mohammad Samragh, and Farinaz Koushanfar. ReBNet: Residual binarized neural network. In *IEEE International Symposium on Field-Programmable Custom Computing Machines*, 2018.

Boris Ginsburg, Sergei Nikolaev, and Paulius Micikevicius. Training of deep networks with half-precision float. In *Nvidia GPU Technology Conference*, 2017.

Xavier Glorot and Yoshua Bengio. Understanding the difficulty of training deep feedforward neural networks. In *International Conference on Artificial Intelligence and Statistics*, 2010.

Benjamin Graham. Low-precision batch-normalized activations. *arXiv preprint arXiv:1702.08231*, 2017.

Audrunas Gruslys, Rémi Munos, Ivo Danihelka, Marc Lanctot, and Alex Graves. Memory-efficient backpropagation through time. In *Advances in Neural Information Processing Systems*, 2016.

Xiangyu He, Zitao Mo, Ke Cheng, Weixiang Xu, Qinghao Hu, Peisong Wang, Qingshan Liu, and Jian Cheng. Proxybnn: Learning binarized neural networks via proxy matrices. In *European Conference on Computer Vision*, 2020.

Koen Helwegen, James Widdicombe, Lukas Geiger, Zechun Liu, Kwang-Ting Cheng, and Roeland Nusselder. Latent weights do not exist: Rethinking binarized neural network optimization. In *Advances in Neural Information Processing Systems*, 2019.

Elad Hoffer, Ron Banner, Itay Golan, and Daniel Soudry. Norm matters: Efficient and accurate normalization schemes in deep networks. In *Advances in Neural Information Processing Systems*, 2018.

Mark Horowitz. Computing’s energy problem (and what we can do about it). In *International Solid-State Circuits Conference*, 2014.

Diederik P. Kingma and Jimmy Ba. Adam: A method for stochastic optimization. In *International Conference on Learning Representations*, 2015.

Liangzhen Lai, Naveen Suda, and Vikas Chandra. Deep convolutional neural network inference with floating-point weights and fixed-point activations. In *International Conference on Machine Learning*, 2017.

Xiaofan Lin, Cong Zhao, and Wei Pan. Towards accurate binary convolutional neural network. In *Conference on Neural Information Processing Systems*, 2017.

Zechun Liu, Baoyuan Wu, Wenhan Luo, Xin Yang, Wei Liu, and Kwang-Ting Cheng. Bi-Real Net: Enhancing the performance of 1-bit CNNs with improved representational capability and advanced training algorithm. In *European Conference on Computer Vision*, 2018.

Zechun Liu, Zhiqiang Shen, Marios Savvides, and Kwang-Ting Cheng. ReActNet: Towards precise binary neural network with generalized activation functions. In *European Conference on Computer Vision*, 2020.

Brendan McMahan, Eider Moore, Daniel Ramage, Seth Hampson, and Blaise Agüera y Arcas. Communication-efficient learning of deep networks from decentralized data. In *International Conference on Artificial Intelligence and Statistics*, 2017.

Paulius Micikevicius, Sharan Narang, Jonah Alben, Gregory Diamos, Erich Elsen, David Garcia, Boris Ginsburg, Michael Houston, Oleksii Kuchaiev, Ganesh Venkatesh, and Hao Wu. Mixed precision training. In *International Conference on Learning Representations*, 2018.

Haotong Qin, Ruihao Gong, Xianglong Liu, Xiao Bai, Jingkuan Song, and Nicu Sebe. Binary neural networks: A survey. *Pattern Recognition*, 105, 2020.

Eyyüb Sari, Mouloud Belbahri, and Vahid P. Nia. How does batch normalization help binary training. *arXiv preprint arXiv:1909.09139*, 2019.

Nimit S. Sohoni, Christopher R. Aberger, Megan Leszczynski, Jian Zhang, and Christopher Ré. Low-memory neural network training: A technical report. *arXiv preprint arXiv:1904.10631*, 2019.

Yaman Umuroglu, Nicholas J. Fraser, Giulio Gambardella, Michaela Blott, Philip H. W. Leong, Magnus Jahre, and Kees Vissers. FINN: A framework for fast, scalable binarized neural network inference. In *ACM/SIGDA International Symposium on Field-Programmable Gate Arrays*, 2017.

Yaman Umuroglu, Yash Akhauri, Nicholas J. Fraser, and Michaela Blott. LogicNets: Co-designed neural networks and circuits for extreme-throughput applications. In *International Conference on Field-Programmable Logic and Applications*, 2020.

Erwei Wang, James J. Davis, Peter Y. K. Cheung, and George A. Constantinides. LUTNet: Rethinking inference in FPGA soft logic. In *IEEE International Symposium on Field-Programmable Custom Computing Machines*, 2019a.

Erwei Wang, James J. Davis, Ruizhe Zhao, Ho-Cheung Ng, Xinyu Niu, Wayne Luk, Peter Y. K. Cheung, and George A. Constantinides. Deep neural network approximation for custom hardware: Where we've been, where we're going. *ACM Computing Surveys*, 52(2), 2019b.

Erwei Wang, James J. Davis, Peter Y. K. Cheung, and George A. Constantinides. LUTNet: Learning FPGA configurations for highly efficient neural network inference. *IEEE Transactions on Computers*, 2020.

Naigang Wang, Jungwook Choi, Daniel Brand, Chia-Yu Chen, and Kailash Gopalakrishnan. Training deep neural networks with 8-bit floating point numbers. In *Advances in Neural Information Processing Systems*, 2018.

Wei Wen, Cong Xu, Feng Yan, Chunpeng Wu, Yandan Wang, Yiran Chen, and Hai Li. TernGrad: Ternary gradients to reduce communication in distributed deep learning. In *Advances in Neural Information Processing Systems*, 2017.

Ashia C. Wilson, Rebecca Roelofs, Mitchell Stern, Nati Srebro, and Benjamin Recht. The marginal value of adaptive gradient methods in machine learning. In *Advances in Neural Information Processing Systems*, 2017.

Shuang Wu, Guoqi Li, Feng Chen, and Luping Shi. Training and inference with integers in deep neural networks. In *International Conference on Learning Representations*, 2018a.

Shuang Wu, Guoqi Li, Lei Deng, Liu Liu, Dong Wu, Yuan Xie, and Luping Shi. l_1 -norm batch normalization for efficient training of deep neural networks. *IEEE Transactions on Neural Networks and Learning Systems*, 30(7), 2018b.

Shuchang Zhou, Zekun Ni, Xinyu Zhou, He Wen, Yuxin Wu, and Yuheng Zou. DoReFa-Net: Training low bitwidth convolutional neural networks with low bitwidth gradients. *arXiv preprint arXiv:1606.06160*, 2016.

Appendix

A Convergence Rate Analysis

A.1 Theoretical Support

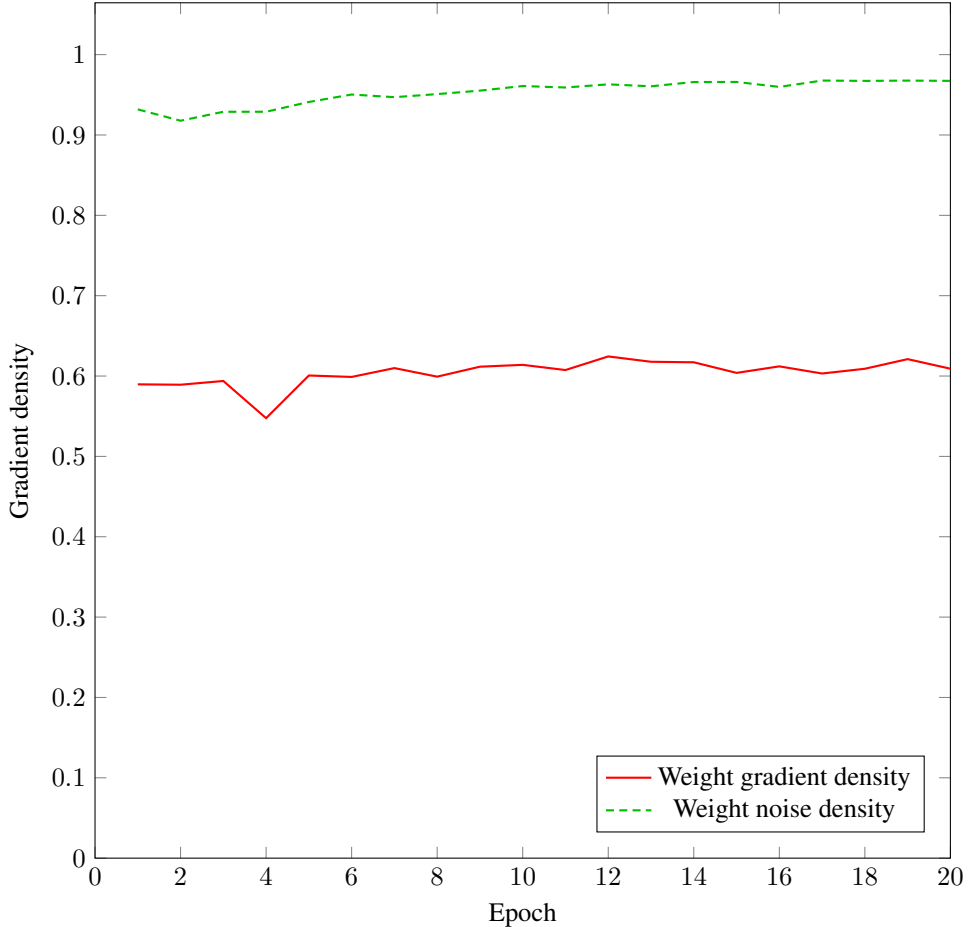


Figure 3: Weight density of the sixth convolutional layer of BinaryNet trained with `bool` weight and `po2_5` activation gradients using Adam and the CIFAR-10 dataset.

Bernstein et al. [2018] proved that training non-binary networks with binary weight gradients may result in similar convergence rates to those of unquantized training if *weight gradient density* $\phi([\mu(\partial\mathbf{W}_1), \dots, \mu(\partial\mathbf{W}_S)]^T)$ and *weight noise density* $\phi([\sigma(\partial\mathbf{W}_1), \dots, \sigma(\partial\mathbf{W}_S)]^T)$ remain within an order of magnitude throughout a training run. Here, S is the training step size and $\phi(\bullet) = \frac{\|\bullet\|_1^2}{N\|\bullet\|_2^2}$ denotes the density function of an N -element vector.

We repeated Bernstein et al.’s evaluation with our proposed gradient quantization applied during BinaryNet training with the CIFAR-10 dataset using Adam and hyperparameters as detailed in Appendix B.1. The results of this experiment can be found in Figure 3. We chose to show the densities of BinaryNet’s sixth convolutional layer since this is the largest layer in the network. Each batch of inputs was trained using quantized gradients $\partial\hat{\mathbf{W}}$ and $\partial\hat{\mathbf{Y}}$. The trained network was then evaluated using the same training data to obtain the `float32` (unquantized) $\partial\mathbf{W}$ used to plot the data shown in Figure 3. We found that the weight gradient density ranged from 0.55–0.62, and weight noise density 0.92–0.97, therefore concluding that our quantization method may result in similar convergence rates to the unquantized baseline.

It should be noted that Bernstein et al.’s derivations assumed the use of smooth objective functions. Although the forward propagation of BNNs is not smooth due to binarization, their training functions still assume smoothness due to the use of straight-through estimation.

A.2 Empirical Support

Figures 4, 5, 6 and 7 contain the training accuracy curves of all experiments conducted for this work. The curves of the standard and our proposed training methods are broadly similar, supporting the conclusion from Appendix A.1 that our proposals do not induce significant convergence rate change.

B Experimental Setup

B.1 Small-Scale Datasets

We used the development-based learning rate scheduling approach proposed by Wilson et al. [2017] with an initial learning rate η of 0.001 for all optimizers except for SGD with momentum, for which we used 0.1. We used batch size $B = 100$ for all except for Bop, for which we used $B = 50$ as recommended by Helwegen et al. [2019]. MNIST and CIFAR-10 were trained for 1000 epochs; SVHN for 200.

B.2 ImageNet

Finding development-based learning rate scheduling to not work well with ResNetE-18, we resorted to the fixed decay schedule described by Bethge et al. [2019]. η began at 0.001 and decayed by a factor of 10 at epochs 70, 90 and 110. We trained for 120 epochs with $B = 4096$.

C Robustness of BNN Backward Propagation to Approximation

To illustrate that BNNs are more robust to approximation in backward propagation than their higher-precision counterparts, we applied our method to both BNNs and float32 networks, with identical topologies and hyperparameters. Results of those experiments are shown in Table 6, in which significantly higher accuracy degradation was observed for the non-binary networks, as expected.

Table 6: Test accuracy of non-binary and BNNs using standard and proposed training approaches with Adam. Results for our training approach applied to the former are included for reference only; we do not advocate for its use with non-binary networks.

Model	Dataset	Top-1 test accuracy						
		Standard training		Reference training		Proposed training		
		NN (%) ¹	BNN (%)	Δ (pp)	NN (%) ¹	Δ (pp) ²	BNN (%)	Δ (pp) ³
MLP	MNIST	98.22	98.24	0.02	89.98	-8.24	96.83	-1.41
CNV	CIFAR-10	86.37	82.67	-3.70	69.88	-16.49	82.31	-0.36
CNV	SVHN	97.30	96.37	-0.93	79.44	-17.86	94.22	-2.15
BinaryNet	CIFAR-10	88.20	89.81	1.61	76.56	-11.64	88.36	-1.45
BinaryNet	SVHN	96.54	97.40	0.86	85.71	-10.83	95.78	-1.62

¹ Non-binary neural network.

² Baseline: non-binary network with standard training.

³ Baseline: BNN with standard training.

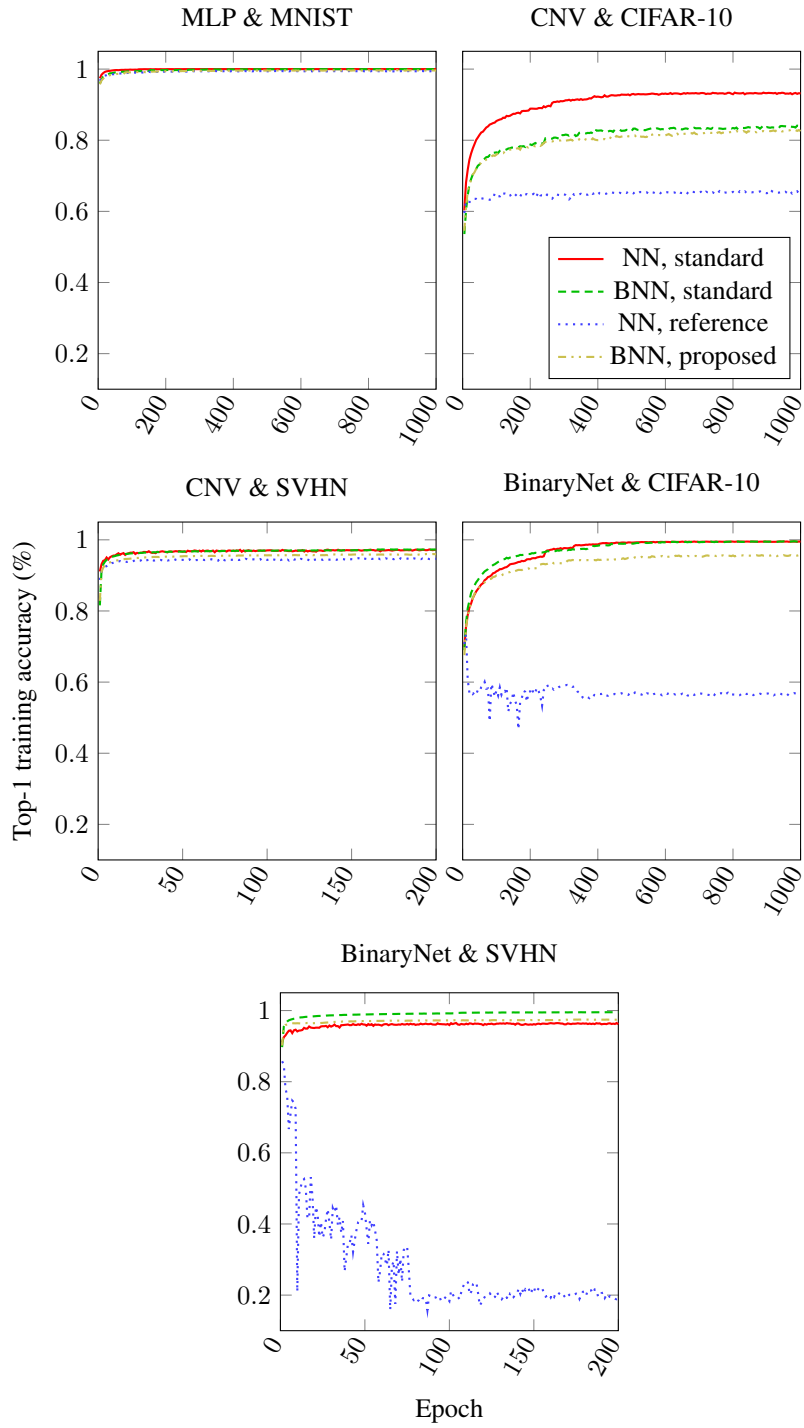


Figure 4: Achieved training accuracy over time for experiments reported in Table 3.

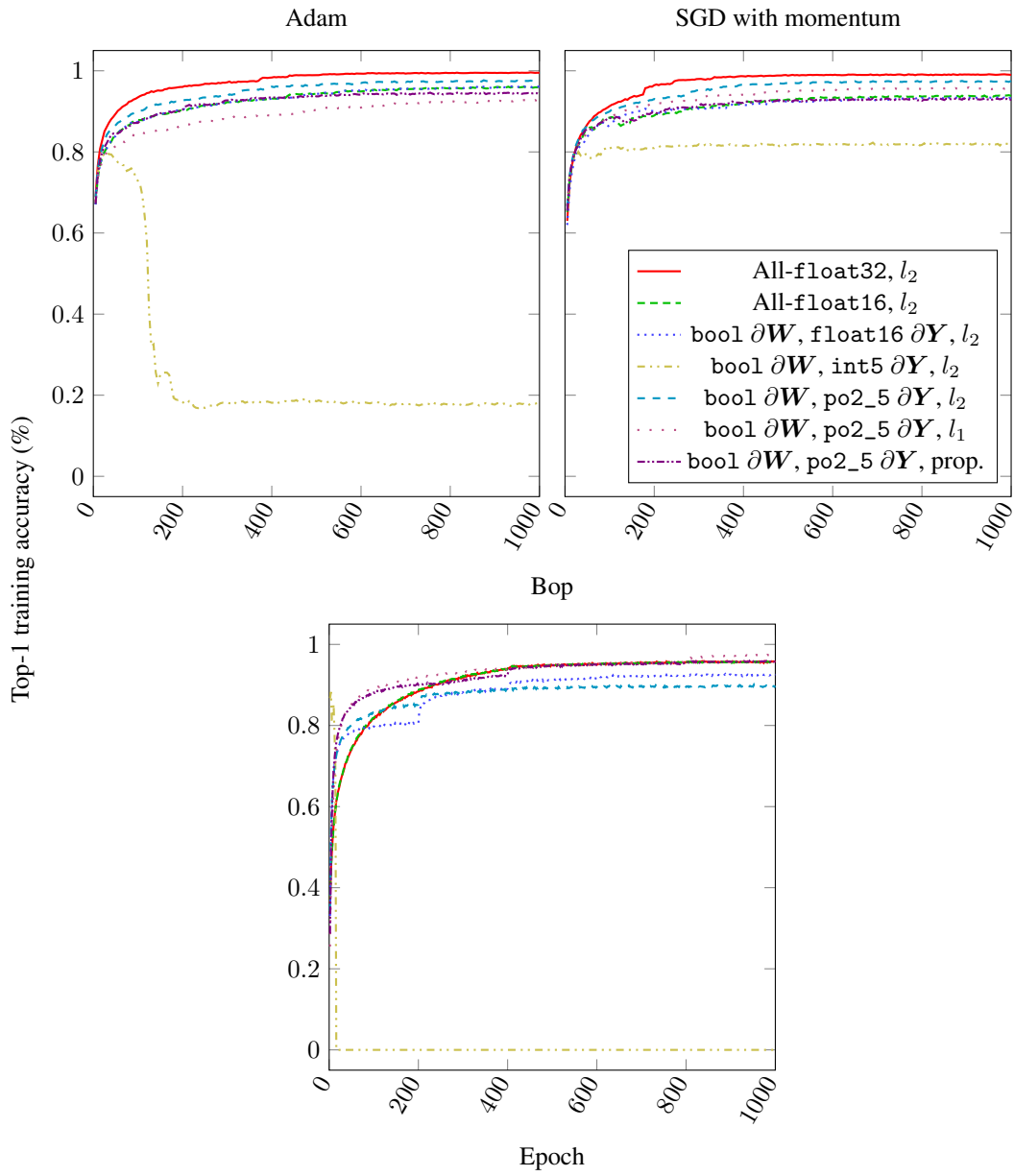


Figure 5: Achieved training accuracy over time for experiments reported in Table 4.

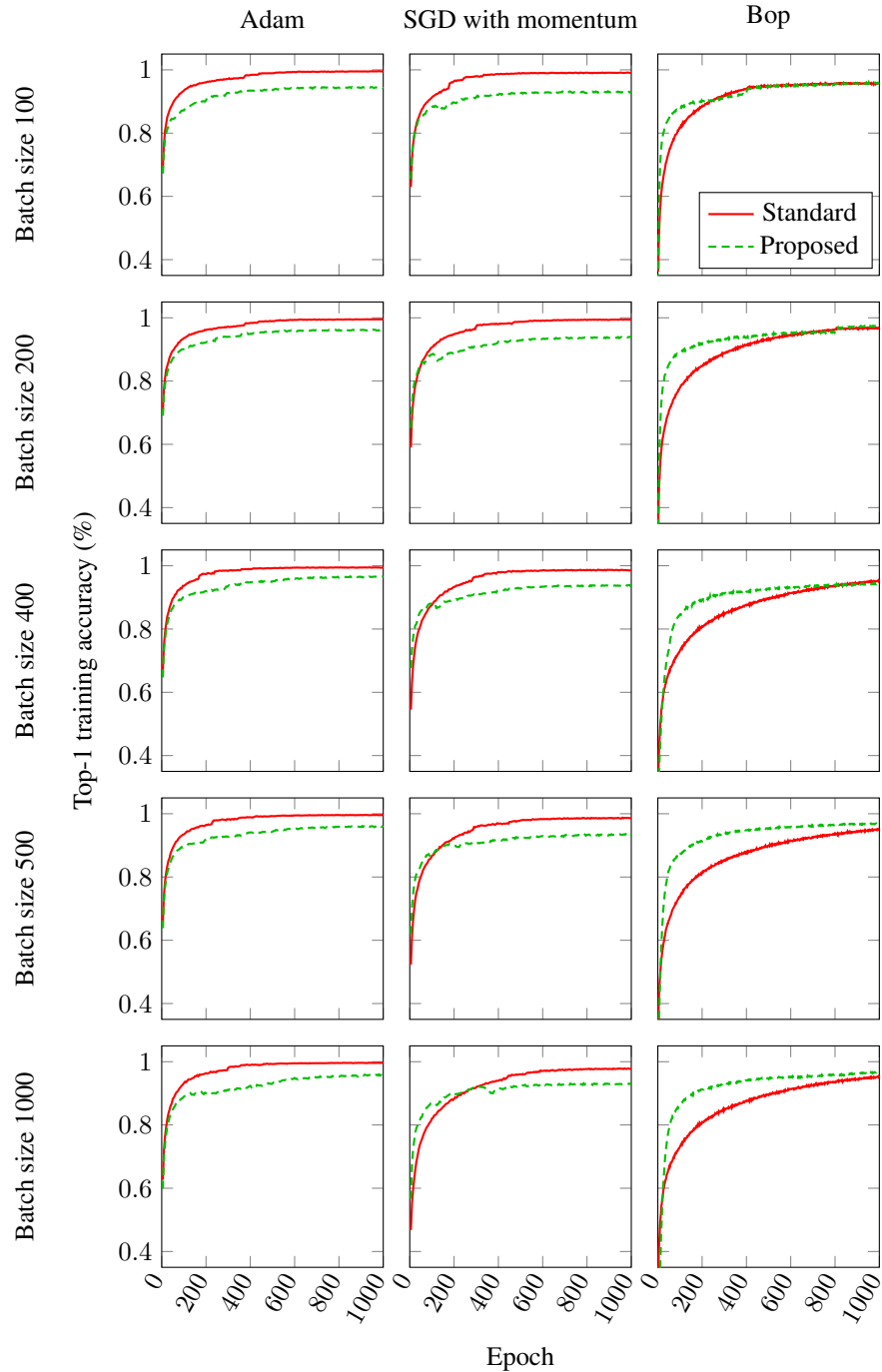


Figure 6: Achieved training accuracy over time for experiments reported in Figure 2.

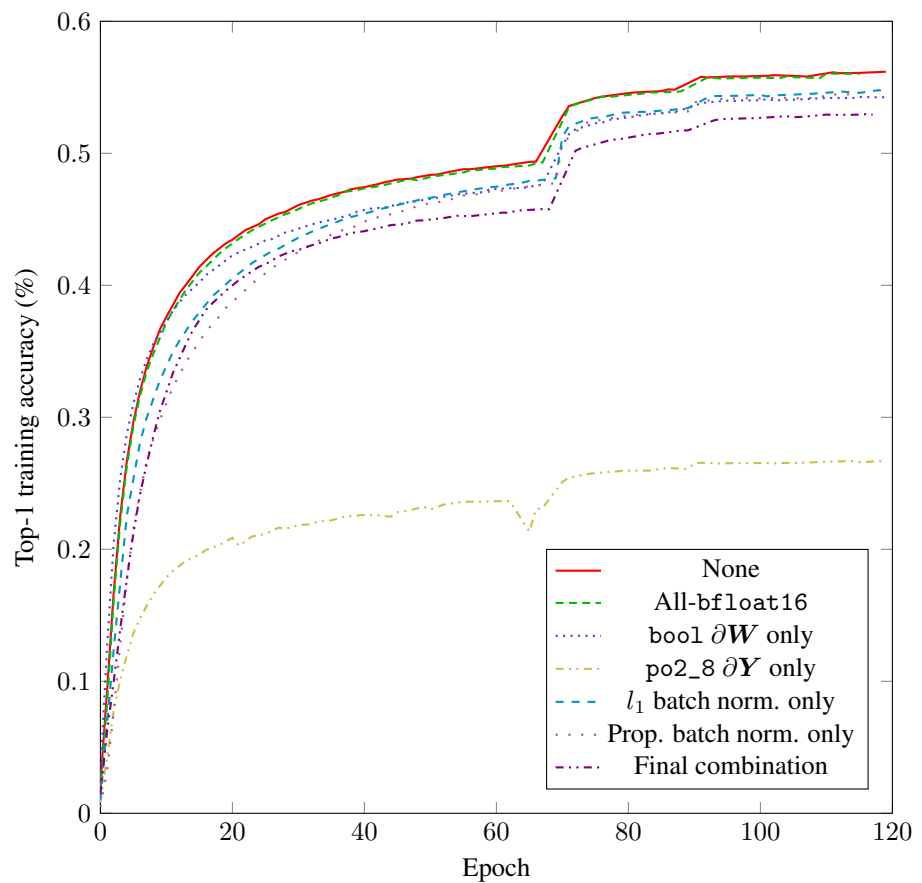


Figure 7: Achieved training accuracy over time for experiments reported in Table 5.